Direct Observation of Excitons and a Continuum of One-Dimensional Mott Insulators: A Reflection-Type Third-Harmonic-Generation Study of Ni-Halogen Chain Compounds

M. Ono,[1] H. Kishida,[1] and H. Okamoto[1,2,*]

[1]*Department of Advanced Materials Science, University of Tokyo, Kashiwa, Chiba 277-8561, Japan*

[2]*Correlated Electron Research Center (CERC), National Institute of Advanced Industrial Science and Technology (AIST), Tsukuba 305-8564, Japan*

(Received 29 July 2004; published 16 August 2005)

The third-harmonic-generation (THG) spectrum was measured for a NiBr-chain compound, which is a one-dimensional Mott insulator, in a reflection configuration. A sharp peak and a shoulder structure in the THG spectrum are attributed to three-photon resonance to an exciton and a continuum, respectively. The band-edge energy, the exciton binding energy, and the spectral weights for the exciton and the continuum were determined from comparative studies of linear absorption, THG, and electroreflectance spectra. The excitonic effect is more pronounced in the NiCl chain than in the NiBr chain.

DOI: 10.1103/PhysRevLett.95.087401 PACS numbers: 78.67.−n, 42.65.Ky, 71.35.Cc

In one-dimensional (1D) semiconductors, excitons play a dominant role in defining optical properties. The binding energy, E_b, of the lowest-energy exciton in 1D systems becomes extremely large due to the singularity of the 1D Coulomb potential. In fact, E_b reaches 0.5 eV in a polydiacetylene Peierls insulator [1] and 1 eV in a polysilane band insulator [2]. In these materials, the oscillator strength is concentrated in the lowest-energy exciton and the transition to the continuum cannot be distinguished in the absorption spectrum. Such a concentration of the oscillator strength in the exciton enhances nonlinear optical (NLO) response [3].

Recently, it was reported, based on electroreflectance (ER) studies, that 1D Mott insulators (MIs) such as Ni-halogen(X) chain and CuO chain compounds show large third-order nonlinear susceptibility $\chi^{(3)}$ [4]. ER studies revealed that $\mathrm{Im}\chi^{(3)}(-\omega; 0, 0, \omega)$ in the 1D MIs was 1–2 orders of magnitude larger than in 1D Peierls and band insulators. To understand the large NLO response in the 1D MIs, it is necessary to take excitonic effects into account. Excitonic nature of the 1D MIs, however, should be different from that of 1D Peierls and band insulators, since on-site Coulomb repulsion U, which is much larger than E_b, works between electrons. According to the half-filled, extended Hubbard model with large U, an exciton is stabilized only when the intersite Coulomb energy V is larger than twice the transfer energy t [5,6]. Therefore, in the 1D MIs, it is important to discriminate contributions of an exciton and a continuum to NLO responses. For this purpose, the most effective method is third-harmonic-generation (THG) spectroscopy. In this method, we can evaluate not only absolute values of $|\chi^{(3)}(-3\omega; \omega, \omega, \omega)|$, but also energy positions of both excitons and a continuum via multiphoton resonant processes. Hereafter, $\chi^{(3)}(-3\omega; \omega, \omega, \omega)$ is simply written as $\chi^{(3)}$.

THG spectroscopy is usually performed in the transmission (T-THG) configuration. A thin film is indispensable to avoid absorption of TH lights. For the CuO chains, growth of thin films is possible by a laser ablation technique. In fact, we measured their $|\chi^{(3)}|$ spectra and showed that $|\chi^{(3)}|$ reaches 10^{-9} esu in Sr_2CuO_3 [7]. The roles of excitons and a continuum on the NLO responses have, however, not yet been clarified. In the NiX chains, $\mathrm{Im}\chi^{(3)}(-\omega; 0, 0, \omega)$ is much larger than in the CuO chains, and the excitonic effect will be more important because of the strong 1D nature of the electronic structures [8]. Therefore, THG measurements on the NiX chains are required. However, their thin films have never been obtained. An alternative method to measure $\chi^{(3)}$ is to detect THG in the reflection (R-THG) configuration (Fig. 1) [9]. So far, no R-THG measurements have been conducted to determine $|\chi^{(3)}|$ over a wide energy region.

In this Letter, we report the $|\chi^{(3)}|$ spectra obtained by R-THG for three NiX chains, $[Ni(chxn)_2Br]Br_2$, $[Ni(chxn)_2Cl]Cl_2$, and $[Ni(chxn)_2Cl](NO_3)_2$ (chxn = cyclohexanediamine). Hereafter, they are abbreviated as Ni-Br-Br, Ni-Cl-Cl, and Ni-Cl-NO_3. By scrutinizing the $|\chi^{(3)}|$ spectra as well as the linear and $\mathrm{Im}\chi^{(3)}(-\omega; 0, 0, \omega)$ spectra, we have succeeded in (1) determining the band edge and E_b, (2) determining the spectral weights of the excitons and the continuum, and (3) clarifying contributions of the nearly degenerate odd and even excitons and the continuum to the NLO response.

Single crystals of the Ni compounds were grown by an electrochemical method [10]. In the NiX chains, X^- and Ni^{3+} ions are arranged alternately to form a 1D electronic structure. A large U on Ni opens a Mott-Hubbard gap in the

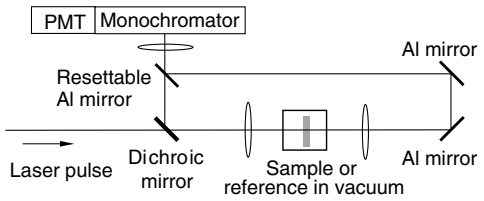

FIG. 1. Experimental setup for the R-THG spectroscopy.

d band [8]. Strong absorption due to charge transfer (CT) transition from the X p band to the Ni d upper-Hubbard band are observed at 1–2 eV as seen in ϵ_2 (imaginary part of dielectric constant) spectra of Figs. 2(a) and 3(a). Among the NiX chains, the pd hybridization, characterized by t_{pd}^2/Δ, is larger in the NiBr chain than in the NiCl chain. Here, t_{pd} is the transfer energy between Ni d_{z^2} and X p_z orbital, and Δ the CT energy. In the NiCl chains, the Ni-Cl distance is smaller in Ni-Cl-Cl than in Ni-Cl-NO_3, leading to the larger t_{pd} in Ni-Cl-Cl. They suggest that the excitonic effect decreases in the order of Ni-Cl-NO_3 > Ni-Cl-Cl > Ni-Br-Br [11].

The experimental setup for the R-THG spectroscopy is shown in Fig. 1. As the excitation light source, we used a Q-switched Nd:YAG laser and optical parametric oscillator with a duration of 6 ns for 0.6–1.2 eV and a Ti:sapphire regenerative amplifier and optical parametric amplifier with a duration of 130 fs for 0.4–0.7 eV. A polarized laser pulse was incident on the sample and TH light in a backward direction was reflected by a dichroic mirror and detected by a photomultiplier tube (PMT). For the quantitative evaluation of $|\chi^{(3)}|$, we used $SrTiO_3$ (STO) as a reference. The $|\chi^{(3)}|$ spectrum of STO was determined in T-THG by using the Maker fringe method [12], in which quartz was used as a reference. We can obtain $|\chi^{(3)}|$ of the sample from the following relation [9]:

$$|\chi^{(3)}| = |\chi_r^{(3)}| \left| \frac{(1+n_s^{3\omega})(n_s^{\omega}+n_s^{3\omega})}{(1+n_r^{3\omega})(n_r^{\omega}+n_r^{3\omega})} \right| \sqrt{\frac{I_s}{I_r}}. \quad (1)$$

Here, I is the R-THG intensity, $n^{\omega}(n^{3\omega})$ is the refractive index for the incident (TH) light, and the subscripts s and r stand for sample and reference, respectively. The refractive indexes are obtained from the Kramers-Kronig analysis of the polarized reflectivity spectra.

In Fig. 2(b), the $|\chi^{(3)}|$ spectrum of Ni-Br-Br is shown as a function of the incident photon energy. The max$|\chi^{(3)}|$ is fairly large, reaching 10^{-8} esu. $|\chi^{(3)}|$ has a sharp peak A at 0.42 eV. Its energy is one-third of the peak energy (E_{CT} = 1.27 eV) of ϵ_2; therefore, it is attributable to the three-photon resonance to the odd CT state. In addition, a shoulder structure C at about 0.5 eV and a hump structure B at 0.64 eV were observed. The previous ER study [4,11] suggested that the even CT state is located very close to the odd one. E_{CT} equals double the energy of the structure B. Therefore, we assigned B to the two-photon resonance to the even CT state and simulated $|\chi^{(3)}|$ using a three-level model (3LM) composed of the ground state $|0\rangle$, the odd CT state $|1\rangle$, and the even CT state $|2\rangle$. In the 3LM, the main term of $\chi^{(3)}$ is expressed as [13]

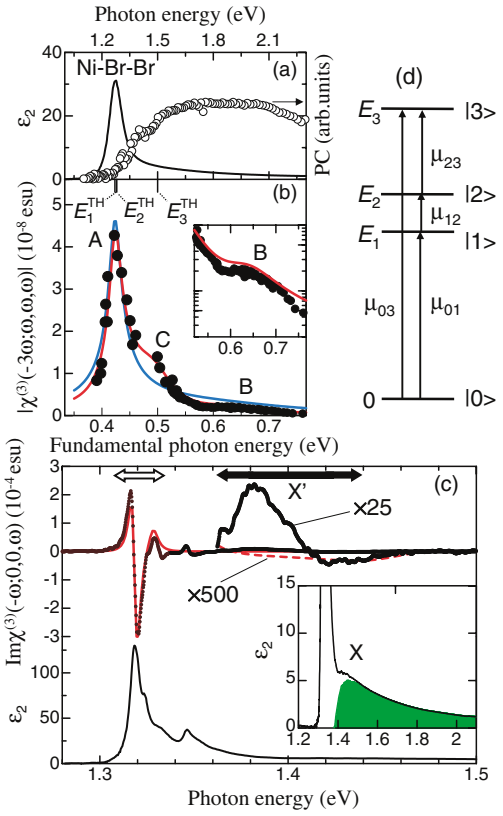

FIG. 2 (color). Linear and nonlinear spectra of Ni-Br-Br. (a) ϵ_2 spectrum at room temperature (RT) and excitation profile of photoconductivity (PC) at 50 K. (b) $|\chi^{(3)}(-3\omega;\omega,\omega,\omega)|$ spectrum at RT (solid circles) and calculated ones by the 3LM (blue line) and the 4LM (red line). $E_1^{TH} - E_3^{TH}$ are the energies of the excited states evaluated by using the 4LM illustrated in (d). (c) ϵ_2 and $\mathrm{Im}\chi^{(3)}(-\omega;0,0,\omega)$ spectra at 4 K. $\mathrm{Im}\chi^{(3)}(-\omega;0,0,\omega)$ above 1.36 eV (bold line) is magnified by a factor of 25. The red broken line shows the calculated spectrum (magnified by a factor of 500) based on the 4LM. The electric field of light and the applied electric field are parallel to the chain axis b.

$$\chi_{\mathrm{main}}^{(3)} = \frac{Ne^4}{\epsilon_0} \frac{\mu_{01}\mu_{12}\mu_{21}\mu_{10}}{(E_1 - E - i\gamma_1)(E_2 - 2E - i\gamma_2)(E_1 - 3E - i\gamma_1)}, \quad (2)$$

where N is the number of Ni per unit volume, and $E_{1,2}(\gamma_{1,2})$ is the energy (damping) of the $|1,2\rangle$ state. μ_{ij} is the dipole moment between $|i\rangle$ and $|j\rangle$. For E_1, γ_1, and μ_{01}, we used the values evaluated by fitting a Lorentzian to the ϵ_2 spectrum. The calculated spectrum is shown as the blue line in Fig. 2(b), which cannot reproduce the structure C and the intensity of B. C cannot be attributed to two-photon resonance to an even state, since double the energy is much lower than E_{CT}. Therefore, we assumed that C is due to a three-photon resonance to another odd state $|3\rangle$. The resultant 4LM is illustrated in Fig. 2(d). In this model, the main term of $\chi^{(3)}$ is given as [13]

$$\chi_{\mathrm{main}}^{(3)} = \frac{Ne^4}{\epsilon_0} \left[\frac{\mu_{01}\mu_{12}\mu_{21}\mu_{10}}{(E_1 - E - i\gamma_1)(E_2 - 2E - i\gamma_2)(E_1 - 3E - i\gamma_1)} + \frac{\mu_{01}\mu_{12}\mu_{23}\mu_{30}}{(E_1 - E - i\gamma_1)(E_2 - 2E - i\gamma_2)(E_3 - 3E - i\gamma_3)} \right]. \quad (3)$$

By using this model, we calculated $|\chi^{(3)}|$ [the red line in Fig. 2(b)], which reproduces well the B and C structures as well as A. The energies E_i^{TH} ($i = 1$–3) are indicated in Fig. 2(b). It can be seen that $|1\rangle$ and $|2\rangle$ are almost degenerate ($\Delta E_{12}^{\mathrm{TH}} = E_2^{\mathrm{TH}} - E_1^{\mathrm{TH}} = 10$ meV), while $|3\rangle$ is located at an energy much higher than E_1^{TH} and E_2^{TH} ($\Delta E_{13}^{\mathrm{TH}} = E_3^{\mathrm{TH}} - E_1^{\mathrm{TH}} \approx 200$ meV). The obtained parameters $\Delta E_{12}^{\mathrm{TH}}$, $\Delta E_{13}^{\mathrm{TH}}$ and $|\mu_{01}\mu_{12}|$, $|\mu_{23}\mu_{30}|$ are plotted in Fig. 4. The fitting reveals that $|\mu_{01}\mu_{12}| > |\mu_{23}\mu_{30}|$, and $\mu_{23}\mu_{30}$ is opposite in sign to $\mu_{01}\mu_{12}$. In this case, the $\mu_{01}\mu_{12}\mu_{21}\mu_{10}$ term interferes with the $\mu_{01}\mu_{12}\mu_{23}\mu_{30}$ term in the region of the two-photon resonance to $|2\rangle$. It results in the suppression of the structure B.

Next, let us discuss the excitonic effect. In Fig. 2(a), we plotted the excitation profile of photoconductivity (PC) (open circles) previously reported [11]. The PC is very low at E_1^{TH} and E_2^{TH}, but increases with energy and is almost saturated at E_3^{TH}. This indicates that $|1\rangle$ and $|2\rangle$ are excitonic states, while $|3\rangle$ corresponds to the continuum. In general, electric-field effects on the reflectivity spectra of excitons and a continuum are different from each other. In this study, the ER measurements were performed at 4 K to eliminate spectral broadening. Details of the ER method and the procedures to derive $\mathrm{Im}\chi^{(3)}(-\omega; 0, 0, \omega)$ were reported elsewhere [4,11]. The ϵ_2 and $\mathrm{Im}\chi^{(3)}(-\omega; 0, 0, \omega)$ spectra are presented in Fig. 2(c).

In the ϵ_2 spectrum at 4 K, the main peak at 1.318 eV is accompanied by phonon sidebands. In addition, a broad shoulder X is observed at ~1.4 eV [the inset of Fig. 2(c)]. In $\mathrm{Im}\chi^{(3)}(-\omega; 0, 0, \omega)$, an oscillating structure indicated by the open arrow is observed around the CT peak, which is attributable to the field-induced mixing of the odd and even excitons [11]. In fact, the oscillating structure can be reproduced well by the 3LM (not shown) and the 4LM (red line). The energy difference $\Delta E_{12}^{\mathrm{ER}}$ of the odd and even states is just 10 meV. In addition, a broad $(+, -)$ structure X', indicated by the solid arrow, is observed at ~1.4 eV. Judging from the energy position and the broadened spectral shape, X' and X are attributable to the continuum. The $(+, -)$ structure, however, cannot be reproduced even by the 4LM. The 4LM gives only a small negative component at ~1.4 eV shown by the red broken line. The most plausible origin for X' is the Franz-Keldysh (FK) effect [14]. If we assume that the band edge is located at the energy where $\mathrm{Im}\chi^{(3)}(-\omega; 0, 0, \omega)$ crosses zero (1.41 eV), as in the case of interband transitions in semiconductors [14], E_b of the lowest odd exciton is evaluated to be ~90 meV. $\Delta E_{12}^{\mathrm{ER}}$ and E_b are plotted in Fig. 4.

By assuming multi-Lorentz oscillators for the exciton peak and its phonon sidebands, and subtracting them from ϵ_2, we derived the contribution of the continuum [the green region in the inset of Fig. 2(c)]. By integrating ϵ_2, the spectral weights for the continuum (~48%) and the exciton (~52%) are found to be almost equal. It was theoretically expected in the half-filled Mott-Hubbard system with large U that most of the spectral weight is concentrated on the exciton in the case of $V \gg 2t$ [6]. The comparable spectral weights for the exciton and the continuum suggest that V is close to $2t$ in Ni-Br-Br.

In Fig. 3, THG spectra for the NiCl chains are presented together with ER and PC spectra [11]. The $|\chi^{(3)}|$ spectra cannot be reproduced by the 3LM (not shown) but are reproduced well by the 4LM (red lines). $E_1^{\mathrm{TH}} \sim E_3^{\mathrm{TH}}$ are indicated in Fig. 3, and $\Delta E_{12}^{\mathrm{TH}}$, $\Delta E_{13}^{\mathrm{TH}}$, $|\mu_{01}\mu_{12}|$, and $|\mu_{23}\mu_{30}|$ are plotted in Fig. 4. As shown in Fig. 3(a), PC is negligible at E_1^{TH} and E_2^{TH}, and is still small at E_3^{TH}, suggesting that $|3\rangle$ is also affected by excitonic effects.

In the $\mathrm{Im}\chi^{(3)}(-\omega; 0, 0, \omega)$ spectra in Fig. 3(c), the main part of the oscillating structure can be reproduced by the 3LM (not shown) as well as the 4LM (red line). Scrutiny of the spectra revealed that the negative component in the higher energy region can be explained not by the 3LM (blue line), but by considering the fourth state $|3\rangle$ in the 4LM (red line in the inset). These results further demonstrate that the 4LM is essential for understanding both $|\chi^{(3)}|$ and $\mathrm{Im}\chi^{(3)}(-\omega; 0, 0, \omega)$ spectra. $\Delta E_{12}^{\mathrm{ER}}$ and $\Delta E_{13}^{\mathrm{ER}}$ are plotted in Fig. 4. The PC sharply increases near E_3^{ER}, so that $\Delta E_{13}^{\mathrm{ER}}$ can be a measure of E_b.

As seen in Fig. 4, $\Delta E_{13}^{\mathrm{TH}}$ is much larger than $\Delta E_{13}^{\mathrm{ER}}$ (or E_b). This is because E_3^{TH} and E_3^{ER} reflect the weight center of the continuum and the band edge, respectively. E_b is

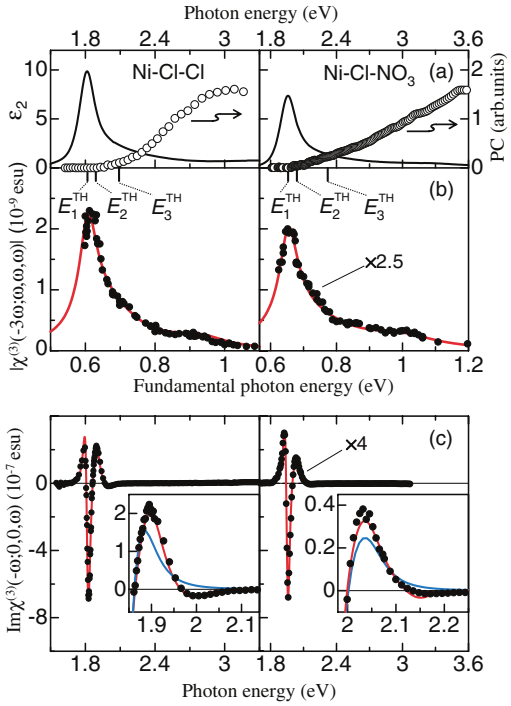

FIG. 3 (color). Linear and nonlinear spectra of Ni-Cl-Cl and Ni-Cl-NO_3. (a) ϵ_2 at RT and the excitation profile of PC (50 K in Ni-Cl-Cl and 150 K in Ni-Cl-NO_3). (b) $|\chi^{(3)}(-3\omega; \omega, \omega, \omega)|$ spectra at RT (solid circles) and calculated ones by the 4LM (red line). (c) $\mathrm{Im}\chi^{(3)}(-\omega; 0, 0, \omega)$ spectra at 77 K and calculated ones by the 3LM (blue line) and the 4LM (red line). The electric field of light and the applied electric field are parallel to b.

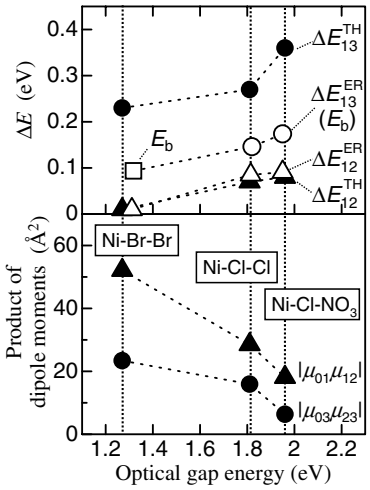

FIG. 4. Parameters evaluated from the analyses of the ϵ_2, $|\chi^{(3)}(-3\omega;\omega,\omega,\omega)|$, and $\mathrm{Im}\chi^{(3)}(-\omega;0,0,\omega)$ spectra for the three NiX chains as a function of gap energy.

larger in the NiCl chains (~200 meV) than in the NiBr chain (~90 meV). This is attributable to the smaller pd hybridization in the NiCl chain, which comes from the larger E_{CT}. The larger excitonic effect explains why the FK effect does not appear in the NiCl chains. It should be noted that the widths of the linear and nonlinear optical spectra in the NiX chains are determined not by the excitonic effect but by the magnitude of the electron-lattice (e-l) interaction [11]. The effect of the e-l interaction is suppressed in the NiBr chain due to the large pd hybridization. It results in sharp spectral widths including the structure C in $|\chi^{(3)}|$. Common to the three NiX chains, $\Delta E_{12}^{\mathrm{TH}}$ (or $\Delta E_{12}^{\mathrm{ER}}$) is much smaller than $\Delta E_{13}^{\mathrm{ER}}$ (or E_b), suggesting that the degeneracy of odd and even excitons is essential in the 1D MIs.

Here, we discuss the material dependence of $\chi^{(3)}$. As a general trend, $\chi^{(3)}$ is enhanced with an increase of the excitonic effect, since oscillator strengths are concentrated on specific transitions. In the NiBr chain, the excitonic effect is relatively small, but is sufficient to concentrate half of the oscillator strength on the lowest exciton. $\chi^{(3)}$ values are mainly determined by the magnitudes of the dipole moments. As seen in Fig. 4, $|\mu_{01}\mu_{12}|$ increases with decreasing E_{CT}, which is due to an increase in the effective pd hybridization. This is the most important origin for the enhancement of $\chi^{(3)}$ in the NiBr chain as compared with the NiCl chains. $\mu_{01}\mu_{12}$ and $\mu_{03}\mu_{23}$ have different signs, so that $\mu_{03}\mu_{23}$ suppresses $|\chi^{(3)}|$ in the two-photon resonance region. However, the robust degeneracy of odd and even excitons provide large μ_{12} and $\mu_{01}\mu_{12}$, overcoming-$\mu_{03}\mu_{23}$, resulting in the enhancement of $|\chi^{(3)}|$.

The 4LM discussed here is analogous to the model used to interpret the NLO response of polysilanes [15] and π-conjugated polymers [16]. In polysilanes, it was reported that the $\chi^{(3)}$ spectra can be well interpreted by taking account of the lowest odd exciton, the second-lowest even exciton, and the third-lowest odd exciton. A similar energy-level structure composed of the odd and even excitons and the continuum has been suggested for the interpretation of the NLO response in π-conjugated polymers [1,17]. Thus, the 4LM is generally quite useful for understanding NLO properties of 1D semiconductors, although the energy position of each excited state and the magnitude of $\chi^{(3)}$ strongly depend on the parameters, U, V, and t as well as on whether the bond alternation exists or not.

In summary, we reported the $|\chi^{(3)}(-3\omega;\omega,\omega,\omega)|$ spectrum of the NiBr-chain compound. A sharp peak and a shoulder structure can be attributed to three-photon resonance for the exciton and the continuum, respectively. The band edge was determined from the $\mathrm{Im}\chi^{(3)}(-\omega;0,0,\omega)$ spectrum at 4 K, indicating that the binding energy of the odd exciton is 90 meV. The spectral weight is equally distributed to the exciton and the continuum, which is attributable to the small excitonic effect in the NiBr chain.

*Corresponding author.
Electronic address: okamotoh@k.u-tokyo.ac.jp

[1] L. Sebastian and G. Weiser, Phys. Rev. Lett. **46**, 1156 (1981).
[2] R. G. Kepler and Z. G. Soos, Phys. Rev. B **43**, 12 530 (1991).
[3] C. Sauteret *et al.*, Phys. Rev. Lett. **36**, 956 (1976).
[4] H. Kishida *et al.*, Nature (London) **405**, 929 (2000).
[5] W. Stephan and K. Penc, Phys. Rev. B **54**, R17 269 (1996); F. B. Gallagher and S. Mazumdar, *ibid.* **56**, 15 025 (1997); Z. Shuai *et al.*, *ibid.* **55**, 15 368 (1997).
[6] F. H. L. Essler *et al.*, Phys. Rev. B **64**, 125119 (2001); E. Jeckelmann, *ibid.* **67**, 075106 (2003).
[7] H. Kishida *et al.*, Phys. Rev. Lett. **87**, 177401 (2001).
[8] H. Okamoto *et al.*, Phys. Rev. B **42**, 10 381 (1990); **54**, 8438 (1996).
[9] C. C. Wang and E. L. Baardsen, Phys. Rev. **185**, 1079 (1969); W. K. Burns and N. Bloembergen, Phys. Rev. B **4**, 3437 (1971); M. Sinclair *et al.*, *ibid.* **38**, 10 724 (1988).
[10] M. Yamashita *et al.*, Mol. Cryst. Liq. Cryst. **256**, 179 (1994).
[11] M. Ono *et al.*, Phys. Rev. B **70**, 085101 (2004).
[12] F. Kajzar *et al.*, J. Appl. Phys. **60**, 3040 (1986).
[13] P. N. Butcher and D. Cotter, *The Elements of Nonlinear Optics* (Cambridge University Press, Cambridge, 1990).
[14] W. Franz, Z. Naturforsch. **13A**, 484 (1958); L. V. Keldysh, Sov. Phys. JETP **34**, 788 (1958).
[15] T. Hasegawa *et al.*, Phys. Rev. Lett. **69**, 668 (1992).
[16] D. Guo *et al.*, Phys. Rev. B **48**, 1433 (1993).
[17] S. Abe *et al.*, Phys. Rev. B **45**, 9432 (1992).